International Journal of Research in Engineering and Science (IJRES)
ISSN (Online): 2320-9364, ISSN (Print): 2320-9356
www.ijres.org Volume 10 Issue 5 ǁ 2022 ǁ PP. 01-08

Numerical study of turbulent flow in gabion open channels

Kasiteropoulou Dorothea*, Papapolymerou George, Spiliotis Xenofon and Christodoulou Dimitrios

Department of Environmental Sciences, University of Thessaly, Larissa, Greece
**Corresponding Author:Dorothea Kasiteropoulou, Assistant Professor, Department of Environmental Sciences, University of Thessaly, Campus Gaiopolis, Larissa, Greece*

Abstract
In order to numerically investigate the flow in open channels with gabion walls a Computational Fluid Dynamical (CFD) model was used. The CFD model is based on the CFX computer package, a high-performance general purpose fluid dynamics program that has been applied to solve a wide-ranging fluid flow problems. The gabion walls are modelled by sand roughness of four different heights: 100mm, 150mm, 200mm and 250mm. Calculations of velocity, pressure, turbulence kinetic energy and eddy viscosity show clearly that the presence of the roughness affects considerably the fluid motion.

Keywords: *Open channel flow, Gabions, CFX, Turbulent flow.*

Date of Submission: 01-05-2022 Date of acceptance: 12-05-2022

I. INTRODUCTION

The turbulent characteristics of the flow are influenced by the type of solid walls. Walls with roughness can affect the flow pattern and the velocity, pressure, turbulence kinetic energy and eddy viscosity values near the bottom and up to the channel in aquatic flows.

Roughness is considered as solid walls with vegetation, gabion walls or/and extruding wall elements. Gabion walls are made of steel cages with wire mesh filled with sand, stones and boulders used to control water fluid flow over solid surfaces. Utmani et al. (2019) used gabion walls as retaining structure in areas with hills. They found that when using gabions in road construction the erosion is effectively controlled because of the high resisting weight and the permeability of the gabions. Nešović et al. (2015) also used rectangular and hexagonal gabions as retaining walls in order to control the stability.

Simac and Bathurst (1997) based on the soil availability and the overall cost investigated experimentally gabion baskets made of geogrid reinforcement and PVC. The gabions were used in the Tellico Plains to Robbinsville highway construction and helped for the stabilization of the road.

Rockfilled gabions are also used for erosion control. Peter et al (1984) used repelling spurs, attracting spurs and deflecting groynes gabions in order to control the removal of exposed particles from the extensive land, stream bank or surfaces and local scour.

Many researchers investigated protection against bed and bank erosion by using vegetated and gabion-lined channels. They found that as the bed and bank material roughness decreases the velocity, the shear stress, the rate of erosion and sediment transport increases. Khalid and Bahzad (2010) also worked on the protection of open channels using gabions and found that the flow rate increases as the gravel mean diameter, the channel side slope and the number of protection layer decreases. Pallavi and Harshith (2018) conducted laboratory experiments in open gabion channel flows and found that the flowing velocity is reduced as it passes through the gabion weir.

Experiments were also performed by Daneshfaraz et al. (2021). They used gabion inclined drops to reduce energy loss and stabillize the hydraulic jump by reducing the Froude number. Crasnell and Akib (2020) investigated the effectiveness of the protection of gabion flume channel. The solid walls were filled with plastic, clothing and stones. The bridge pier scour was reduced due to the gabion effects.

Grupta and Kumar (2020) compared the gabion weirs with solid weirs with respect to the flow characteristics, such as the velocity distribution. They found that in the case of gabion weir flow takes place over the weir as well as through the weir body itself whereas in the solid one it takes place only over the crest of weir.

Biabani et al. (2021) investigated the open flow with embankment gabion weirs. They studied how three different upstream/downstream gabion weirs slopes, filling materials, particle size of the weir and geometrical ration of the height and length of the weir can affect the fluid flow pattern. They found that gabion weirs lead to greater discharge coefficients than those of similar solid weirs.

Experiments require expensive equipment and for that cannot deliver all answers at macroscale channels. At the same time, numerical simulation methods are less expensive and useful for the technical design.

Li and Li (2015) proposed a Double Average Navier-Stokes equation to simulate flows in gabion channels and observed that the zero-place displacement parameter decreases with the increase in the area density of roughness elements. Michalolias et al (2018) investigated both numerically and experimentally the flow in open channels with vegetated solid walls. They observed that the velocity decreases as the vegetation height increases. Low eddy viscosity values were detected in the central part of the channels for all the channel cases.

In this work we numerically investigate the flow in open channels with gabion walls. Velocity, pressure, turbulence kinetic energy and eddy viscosity patterns are presented according to the roughness height and the flow rate.

1.2 MATHEMATICAL MODEL – NUMERICAL SIMULATION

1.2.1 Mathematical Model

The mathematical model of the turbulent flow in this work consists of the Reynolds-Averaged Navier-Stokes (RANS) equations coupled with the k-ε turbulence model. Each primitive flow variable is decomposed to an averaged-in-time part and a fluctuation term. For example, the velocity vector at a point in the flow field is given as the sum of the time-averaged velocity U ! and a time-dependent velocity fluctuation u ! , i.e., we write

$$\vec{U} = \vec{\bar{U}} + \vec{u} \tag{1}$$

The time-averaged velocity vector is defined as

$$\vec{\bar{U}} = \frac{1}{\Delta t}\int_{f}^{f+\Delta t} \vec{U}\, dt \tag{2}$$

where T is a time interval much longer than the characteristic periods of the turbulence fluctuations. The use of mean values (in time) in the conservation equations leads to the Reynolds-Averaged Navier-Stokes (RANS) equations:

$$\frac{\partial \rho}{\partial t} + \nabla \bullet \left(\rho \vec{U}\right) = 0 \tag{3}$$

$$\frac{\partial \rho \vec{U}}{\partial t} + \nabla \bullet \left(\rho \vec{U} \otimes \vec{U}\right) = \nabla \bullet \left(\tau - \rho \overline{\vec{u} \otimes \vec{u}}\right) + \vec{S}_M \tag{4}$$

In Eq. (4), $\rho \overline{\vec{u} \otimes \vec{u}}$ are the Reynolds stresses and τ denotes the stress tensor due to molecular viscosity.

After introducing the concept of an effective viscosity, μeff, the conservation of mass equation is unchanged and the conservation of momentum equation is written as

$$\frac{\partial \rho \vec{U}}{\partial t} + \nabla \bullet \left(\rho \vec{U} \otimes \vec{U}\right) - \nabla \bullet \left(\mu_{eff} \nabla \vec{U}\right) = -\nabla p' + \nabla \bullet \left(\mu_{eff} \nabla \vec{U}\right)^T + \vec{\mathrm{B}} \tag{5}$$

where $\vec{\mathrm{B}}$ the total body force per unit mass, μeff is the effective viscosity and p′ is the modified pressure defined as

$$p' = p + \frac{2}{3}\rho k + \nabla \bullet \vec{U}\left(\frac{2}{3}\mu_{eff} - \zeta\right) \tag{6}$$

In Eq. (6), ζ is the fluid bulk viscosity, ρ is the fluid density and k denotes the turbulent kinetic energy.

The k-ε model is used in this work for the calculation of the turbulent viscosity at each point of the flow field. The k-ε model is a two differential equation model where the effective viscosity is calculated as the sum of turbulent viscosity (μt) and molecular viscosity (μ) i.e.,

$$\mu_{eff} = \mu + \mu_t \tag{7}$$

The turbulent viscosity is computed at each point of the flow field in terms of the turbulence kinetic energy, k, and the turbulence kinetic energy dissipation rate, ε, by the relation

$$\mu_t = C_\mu \rho \frac{k^2}{\varepsilon} \tag{8}$$

where $C_\mu = 0,09$

The required values of k and ε are computed at each point of the turbulent flow field by concurrently solving the following two partial differential equations (Liakopoulos 2010):

$$\frac{\partial(\rho k)}{\partial t} + \nabla \bullet (\rho \vec{U} k) = \nabla \bullet [(\mu + \frac{\mu_t}{\sigma_k})\nabla k] + P_k - \rho\varepsilon \tag{9}$$

$$\frac{\partial(\rho\varepsilon)}{\partial t} + \nabla \bullet (\rho \vec{U} \varepsilon) = \nabla \bullet [(\mu + \frac{\mu_t}{\sigma_\varepsilon})\nabla \varepsilon] + \frac{\varepsilon}{k}(C_{e1} P_k - C_{e2}\rho\varepsilon) \tag{10}$$

where $C_{e1} = 1{,}45$, $C_{e2} = 1{,}90$, $\sigma_k = 1{,}00$, $\sigma_\varepsilon = 1{,}30$ and P_k is the rate of production of turbulence kinetic energy calculated by

$$P_k = \mu_t \nabla \vec{U} \bullet (\nabla \vec{U} + \nabla \vec{U}^T) - \frac{2}{3}\nabla \bullet \vec{U}(3\mu_t \nabla \bullet \vec{U} + \rho k) \tag{11}$$

The ANSYS-CFX computer package is used in this work under the assumption of incompressible flow with constant properties (ρ= constant, μ= constant) and bulk viscosity ζ=0.

1.2.2 Mathematical Model

In order to complete the mathematical model, free slip boundary condition was specified at the free surface. In solid weir flows walls were assumed smooth without slip velocity (no-slip boundary condition) whereas at the gabion channels four different gravel diameter were used simulated as sand grained roughness. A 3-D view of the mesh generated using the ANXYS-CFX preprocessor is shown in figure 1.

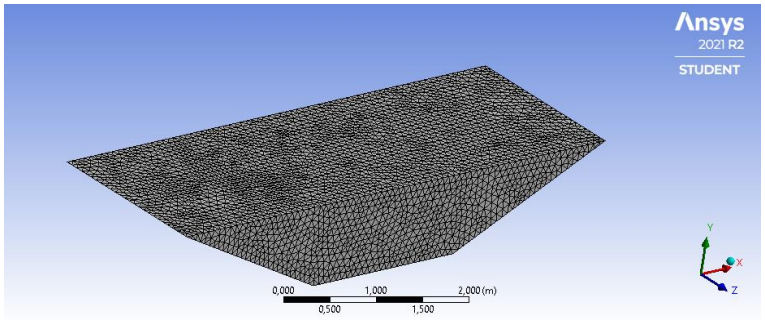

Figure 1: A 3-D view of the mesh

To achieve grid independence, a sequence of mesh designs was used. A maximum edge length equal to 0.08 m and a minimum edge length 0.04 m were chosen in order to resolve the boundary layers formed near all solid surfaces. The grid used for all cases is shown in Table 1. Sensitivity to global quantities, such as mass conservation was helpful in judging approximate convergence of the solutions.

Table 1: Mesh parameters

Discharge (m^3/s)	Number of nodes	Number of tetrahedra	Mean velocity (m/s)	% difference
0.52	24576	129705	0.132513	1,875%
0.52	28595	143924	0.130028	3,556%
0.52	28843	153355	0.125404	5,364%

1.2.3. Channel geometry and modelling

We use a 3D model to study the flow inside a trapezoidal channel of bottom width 2m, top width 6m and flow depth 1m. The gabion channels walls were simulated as gravel bed walls with four different gravel: 100mm, 150mm, 200mm, 250mm. In order to minimize the computational burden we simulated flow by using periodic boundary conditions in the main flow direction. Consequently, our computational domain has a length of 1m. A

3-D (isometric) view of the computational domain is shown in Fig. 2. Five values of discharge were used: Q1=0.52m3/s, Q2=0.79m3/s, Q3=1.58m3/s, Q4=15.41m3/s, Q5=41.96m3/s.

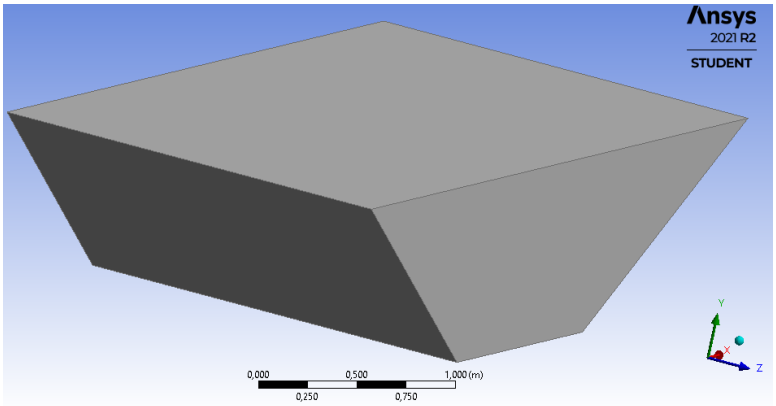

Figure 2: A 3-D view of the channel as modeled in the ANSYS-CFX environment.

II. RESULTS AND DISCUSSION

Various aspects of the computed 3-D velocity field are presented in Figs. 3, 4 and 5. The calculated streamwise velocity and dimensionless velocity for constant discharge is shown in Fig. 3 for the coarse grid (Mesh 3). The dimensionless velocity is useful when comparing the computational results obtained with channelflows of different gravel bed roughness diameter. The calculated streamwise velocity is presented along the line segment (3, 0, 0.5m) to (3,1,0.5m).

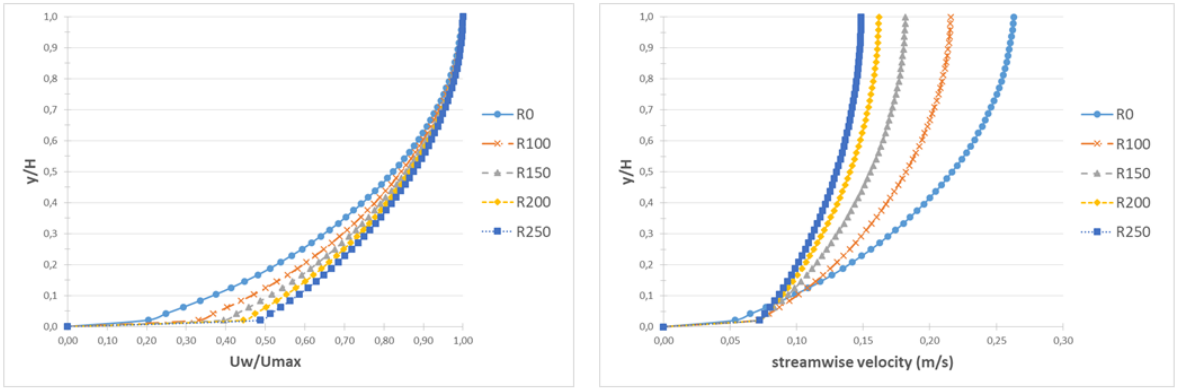

(a) **(b)**

Figure 3: Computed mean velocity profiles along the line segment (3, 0, 0.5m) to (3,1,0.5m) . (a) Dimensional velocity, (b) Non-dimensionalized velocity

We observe that there is an inflection point of the velocity near the bottom with the value depending on the roughness size. In particular, as the gravel diameter increases the dimensionless velocity also increases regarding that the roughness affects the velocity pattern near the wall. Moreover, we observe that as the gravel diameter increases the mean velocity in the middle plane of the channel decreases.

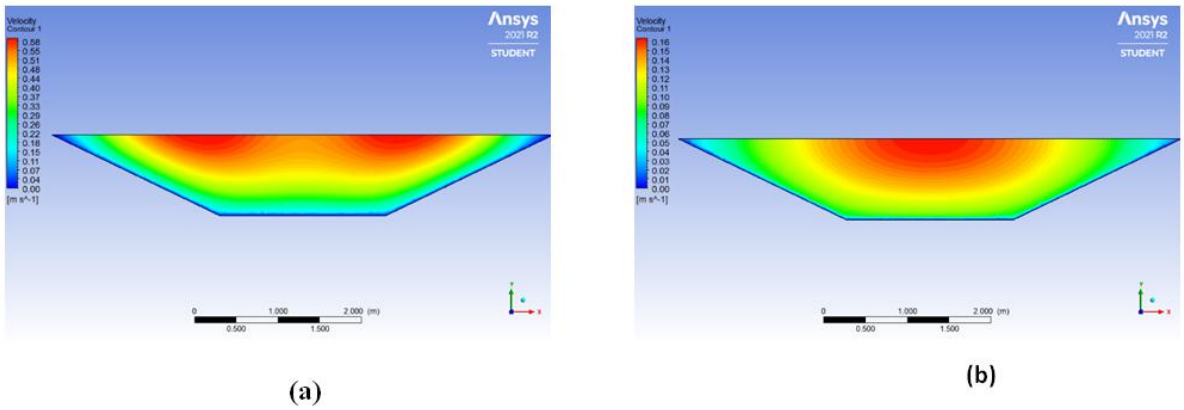

Figure 4: Fluid speed distribution on midplane z=0.5 m for the smooth channel (R0) and (b) for the channel with gravel 250mm (R250). Volume flow rate Q = 1.58 m3/s.

Contour plots of the velocity magnitude for the smooth channel and the channel with gravel diameter 250mm are presented in Figure 4. Again we observe that the gravel effect is important both for the maximum velocity value and also for the fluid speed distribution. However, when comparing smooth and rough solid walls, we note that the velocity profile is significantly affected by the roughness because, sharply lower velocities are observed very close to the rough walls: the velocity near the smooth wall is 0.15m/s while near the rough walls is 0.07m/s (the last can also be observed in Figure 5). The region very close to the wall exhibits a nearly linear velocity profile in the turbulent case, and is completely dominated by viscous effects. It should be noted that in order to accurately resolve the boundary layers, an extremely fine grid must be used and, even if the resolution is adequate, the mean (in time) turbulent velocity profile is not modeled adequately when wall functions are used in the implementation of the k-ε model. For a discussion on k-ε model modification, in order to resolve the boundary layer up to the solid wall, see Liakopoulos (1985).

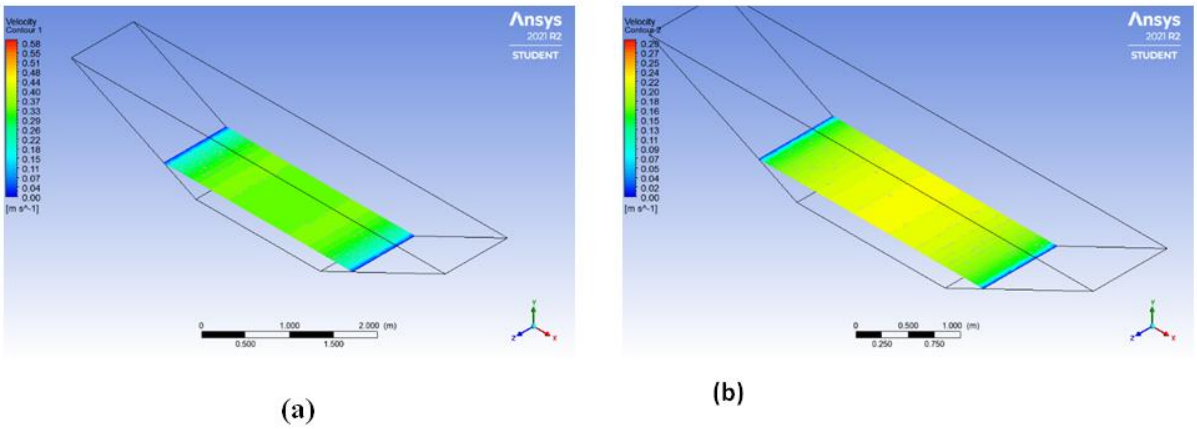

Figure 5: Contour plots of speed velocity at depth y = 0.250 m, for the smooth channel (R0) and (b) for the channel with gravel 250mm (R250). Volume flow rate Q = 1.58 m3/s.

Regarding the computed total mean pressure along the channel presented in Figure 6 we observe that as the volume flow rate increases the effect of the gravel diameter becomes more important. For the same volume flow rate the total mean pressure decreases as the grain diameter increases whereas, for the same roughness the total pressure increases as the volume flow rate also increases. It is important to notice that for large values of flow rate the effect of the roughness in total pressure becomes meaningless. For example, in the cases of volume flow rate Q4=15.41m3/s and Q5=41.96m3/s the dimensionless total pressure is almost equal whereas, for lower volume flow rates there is a big influence.

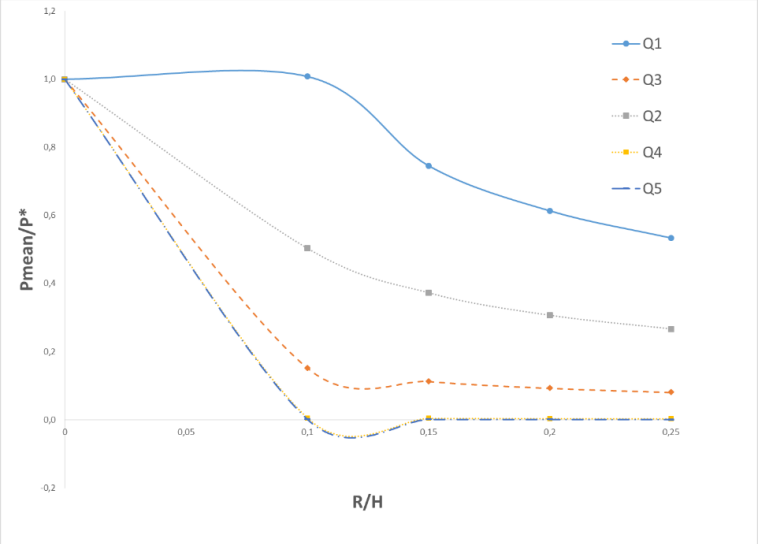

Figure 6: Computed mean dimensional total pressure profiles.

Examining the distribution of the turbulence kinetic energy (Figure 7) and the turbulence kinetic energy value near the bottom (point 3, 0.05, 0.5) and near the top of the channel (point 3, 0.95, 0.5) (Fig.8) we observe that lower values are detected as we move closer to the top of the channel for smooth and rough channels. Near the bottom of the channel higher values are detected in the rough channels and the thickness of the maximum turbulence kinetic energy layer depends on the roughness height. In particular, we observe that as the roughness increases the turbulence kinetic energy decreases near the bottom. According to the top of the channel we observe that the turbulence kinetic energy increases as the roughness height increases.

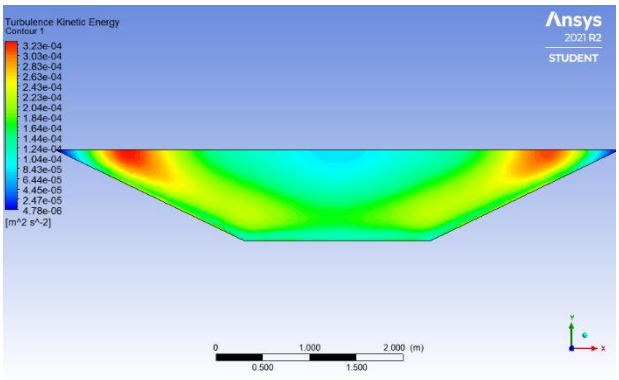

(a)

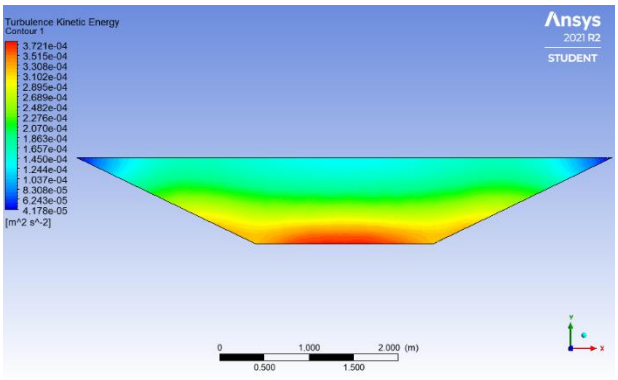

(b)

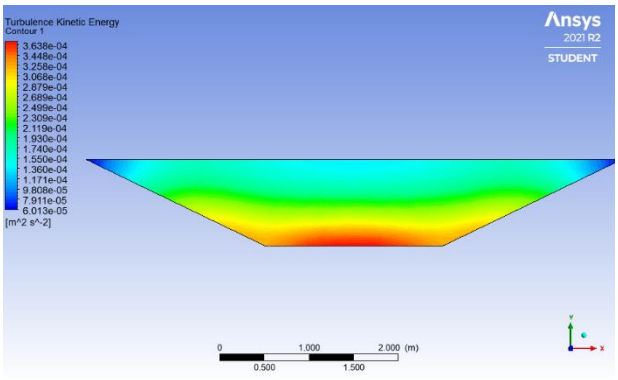

(c)

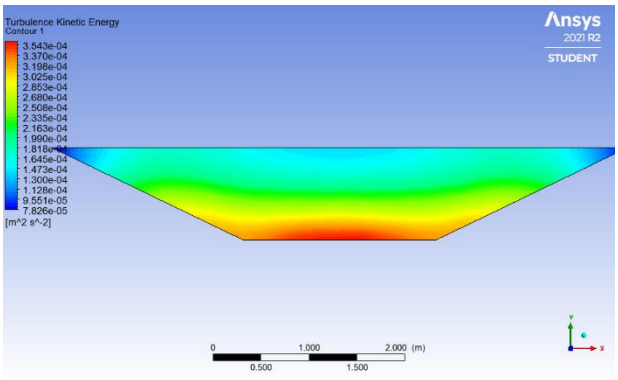

(d)

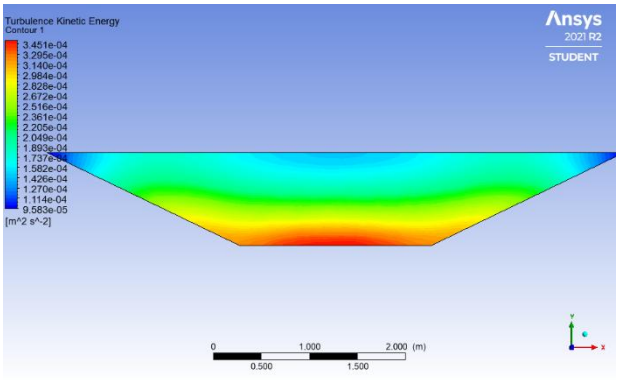

(e)

Figure 7: Turbulence Kinetic energy distribution on midplane z=0.5 m for the smooth channel (R0), and for the channel with gravel (b)100mm, (c)150mm, (d) 200mm, (e)250mm. Volume flow rate Q = 1.58 m3/s.

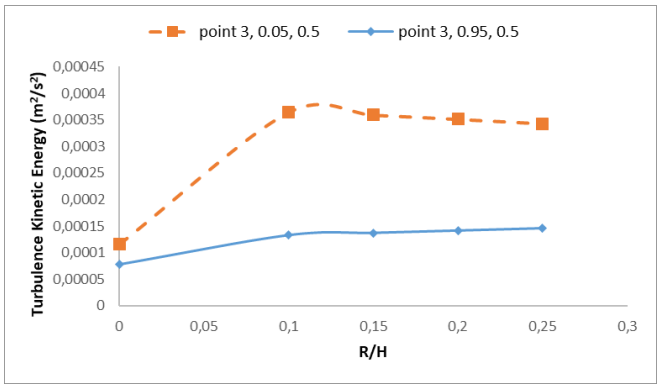

Figure 8: Turbulence Kinetic energy value near the bottom (point 3, 0.05, 0.5) and near the top of the channel (point 3, 0.95, 0.5).Volume flow rate Q = 1.58 m3/s.

In Fig. 9, the eddy viscosity distribution for the channel without gabions and the channel with gabions of gravel diameter 250mm is presented. We observe that low eddy viscosity values, for the smooth channel, are detected in the central part of the channel but they become high in small regions, as shown in Fig.9, at the solid side wallsnear the surface. However, for the rough channel high eddy viscosity values are observed in the central part of the channel throughout the depth of the channel. In Fig. 10, we observe that both near the surface and near the bottom of the channel the eddy viscosity increases as the roughness increases for constant flow rate. Therefore, it is concluded, that thegabion roughness increases eddy viscosity values in a much greater volume of the channel.

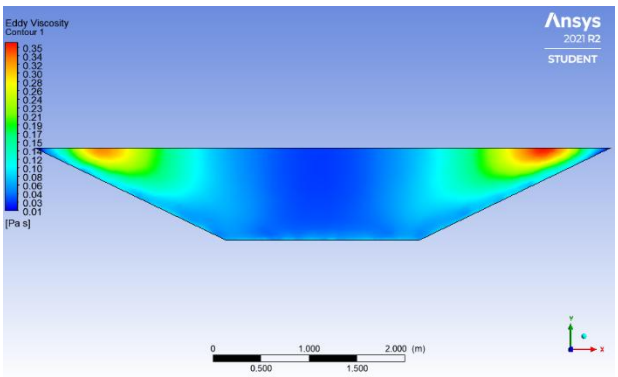

(a)

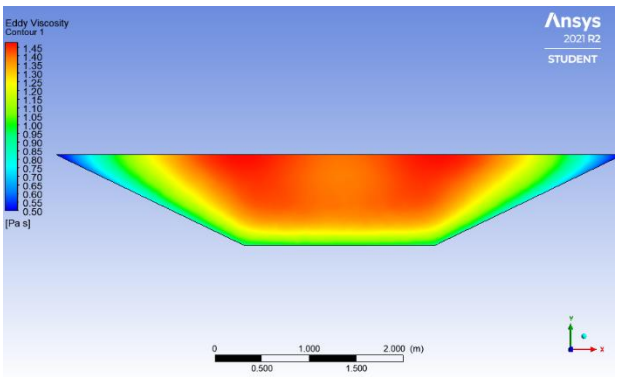

(b)

Figure 9: Eddy viscosity distribution on midplane z=0.5 m for the smooth channel (R0) and (b) for the channel with gravel diameter 250mm (R250). Volume flow rate Q = 1.58 m3/s.

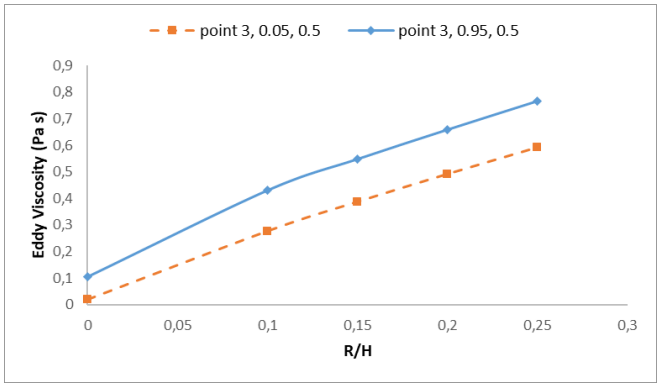

Figure 9:Eddy viscosity value near the bottom (point 3, 0.05, 0.5) and near the top of the channel (point 3, 0.95, 0.5).Volume flow rate Q = 1.58 m3/s.

III. CONCLUSION

In this paper we have presented the simulations of turbulent flow in a trapezoidal open channel whose walls are simulated as gabion walls. The gabion walls are modelled by sand roughness of four different height: 100mm, 150mm, 200mm and 250mm. Calculations of velocity, pressure, turbulence kinetic energy and eddy viscosity show clearly that the presence of the roughness affect considerably the fluid motion. As expected, the rough elements affect the mean velocity inside the channel and near the walls. Near the solid walls, the velocity profile is significantly affected and sharply lower velocities are observed very close to the walls.

REFERENCES

[1]. ANSYS-CFX, Release 11.0 – User Guide.
[2]. Biabani R., Salmasi F., Nouri M. and Abraham J. (2021),"Flow Over Embankment Gabion Weirs in Free Flow Conditions", Research Square, Preprint, DOI: https://doi.org/10.21203/rs.3.rs-572510/v1
[3]. Craswell T and Akib S (2020),"Reducing Bridge Pier Scour Using Gabion MattressesFilled with Recycled and Alternative Materials", Eng 2020, 1, 188–210; doi:10.3390/eng1020013.
[4]. Daneshfaraz R, Bagherzadeh M, Ghaderi A, Francesco S, Asl M (2021),"Experimental Investigation of Gabion Inclined Drops as a Sustainable Solution for Hydraulic Energy Loss", Ain Shams Engineering Journal, 12: 3451-3459.
[5]. Gupta K K and Kumar S (2020),"Flow Characteristics of Gabion Weir for Free Flow Condition – an Experimental Approach", International Journal of Advanced Research in Engineering and Technology (IJARET), Volume 11, Issue 8, August 2020, pp. 889-898.
[6]. Khalid Y T A, Bahzad M A N (2010),"Protection of Open Channels Using Gabions", AL – Rafdain Enginnering Journal, 18: 36-48.
[7]. Liakopoulos A (2010),"Fluid mechanics". Tziolas Publications (in greek).
[8]. Li C-W and Li J. (2015),"DANS model for vegetated open channel flows", Journal of Hydraulic Research, Volume 53, 2015 - Issue 6, pp. 699-713.
[9]. Michalolias N., Keramaris E., Kasiteropoulou D., Liakopoulos A. and Pechlivanidis G. (2018),"Experiments and Numerical Analysis of Flow in an Open Channel with Gravel Bed", Proceedings, Volume 2, 581; doi:10.3390/proceedings2110581, pp. 1-9.
[10]. Nešović I, Paunović S, Petrović M, Ćirić N (2015),"The Stability of Gravity Retaining Structures". 41th Anniversary Faculty of Civil Engineering Subotica, International Conference Contemporary achievements in civil engineering 24. April 2015, Subotica, SERBIA.
[11]. Peter C, Kllngeman, Scott M, Kehe, Yaw A, Owusu (1984) Streambank Erosion Protection and Channel Scour Manipulation Using Rockfill Dikes and Gabions. Department of Civil Engineering, Oregon State University. Water Resources Research Institute Oregon State University Corvallis Oregon.
[12]. Pallavi M, Harshith L (2018), "Open Channel Flow Characteristics using Gabion Weir", International Research Journal of Engineering and Technology, 05 (12): 928-933.
[13]. Simac MR, Bathurst RJ, TW (1997A),"Design of Gabion - Geosynthetic Retaining Walls On the Tellico Plains to Robbinsville Highway", Geosynthetics '97 Conference, California, USA. 105-118.
[14]. Utmani N, Ahmad S, Islam RUI, Abbas M (2019),"Gabion Wall used in Road Construction and Flood Protection Embankment", Journal of Civil Engineering and Environmental Sciences, 5 (1): 001-004, doi: 10.17352/2455-488X.000031